NAVAL POSTGRADUATE SCHOOL
Monterey, California

THESIS

THE ROLE OF PARTICLE CRACKING IN DILATATION DURING TENSILE STRAINING OF A CAST AND THERMOMECHANICALLY PROCESSED 6061 Al -20 VOLUME PERCENT AL_2O_3 METAL MATRIX COMPOSITE

by

Kevin P. Boyle
September, 1996

Thesis Advisor: Terry R. McNelley

Approved for public release; distribution is unlimited.

REPORT DOCUMENTATION PAGE

Form Approved OMB No. 0704-0188

1. AGENCY USE ONLY *(Leave blank)*	2. REPORT DATE September 1996	3. REPORT TYPE AND DATES COVERED Master's Thesis

4. TITLE AND SUBTITLE: **THE ROLE OF PARTICLE CRACKING IN DILATATION DURING TENSILE STRAINING OF A CAST AND THERMOMECHANICALLY PROCESSED 6061 Al - 20 VOLUME PERCENT Al_2O_3 METAL MATRIX COMPOSITE**

5. FUNDING NUMBERS

6. AUTHOR(S) Kevin P. Boyle

7. PERFORMING ORGANIZATION NAME(S) AND ADDRESS(ES)
Naval Postgraduate School
Monterey CA 93943-5000

8. PERFORMING ORGANIZATION REPORT NUMBER

9. SPONSORING/MONITORING AGENCY NAME(S) AND ADDRESS(ES)

10. SPONSORING/MONITORING AGENCY REPORT NUMBER

11. SUPPLEMENTARY NOTES The views expressed in this thesis are those of the author and do not reflect the official policy or position of the Department of Defense or the U.S. Government.

12a. DISTRIBUTION/AVAILABILITY STATEMENT
Approved for public release; distribution is unlimited.

12b. DISTRIBUTION CODE

13. ABSTRACT *(maximum 200 words)* In this work, the dilatation during tensile straining of a cast and thermomechanically processed 6061 Al - Al_2O_3 metal matrix composite (MMC) containing 20 volume percent of Al_2O_3 particles was examined. Standard tensile samples of the MMC and unreinforced 6061 Al were machined. Precise diameter measurements were made of both composite and unreinforced samples prior to and immediately following tensile straining. Tension tests were conducted to various strains as well as to fracture and an extensometer was employed to obtain accurate measurement of the axial strain. The MMC material exhibited a continuously increasing dilatation during tensile straining while the unreinforced 6061 control material deformed plastically at constant volume. Careful metallographic preparation revealed particle cracking in all MMC samples throughout the range of strains examined. A clear trend of increased frequency of particle cracking was observed. Void formation and growth due to cracking of the particles was analyzed and shown to correlate with the dilatation observed during tensile straining of the composite. Linkage of such voids is proposed as the mechanism of crack propagation at failure of the MMC.

14. SUBJECT TERMS Composite Materials, MMCs, DRA, Plastic Deformation, TMP

15. NUMBER OF PAGES 62

16. PRICE CODE

17. SECURITY CLASSIFICATION OF REPORT	18. SECURITY CLASSIFICATION OF THIS PAGE	19. SECURITY CLASSIFICATION OF ABSTRACT	20. LIMITATION OF ABSTRACT
Unclassified	Unclassified	Unclassified	UL

NSN 7540-01-280-5500

Standard Form 298 (Rev. 28)
Prescribed by ANSI Std. 239-18 298-102

Approved for public release; distribution is unlimited

THE ROLE OF PARTICLE CRACKING IN DILATATION DURING TENSILE STRAINING OF A CAST AND THERMOMECHANICALLY PROCESSED 6061 Al - 20 VOLUME PERCENT Al_2O_3 METAL MATRIX COMPOSITE

Kevin P. Boyle
Lieutenant, United States Navy
B.S. Chemistry, University of Illinois, 1990

Submitted in partial fulfillment
of the requirements for the degree of

MASTER OF SCIENCE IN MECHANICAL ENGINEERING

from the

NAVAL POSTGRADUATE SCHOOL

September 1996

Author: _____
Kevin P. Boyle

Approved by: _____
Terry R. McNelley, Thesis Advisor

_____
Terry R. McNelley, Chairman
Department of Mechanical Engineering

ABSTRACT

In this work, the dilatation during tensile straining of a cast and thermomechanically processed 6061 Al- Al_2O_3 metal matrix composite (MMC) containing 20 volume percent of Al_2O_3 particles was examined. Standard tensile test samples of the MMC and unreinforced 6061 Al were machined. Precise diameter measurements were made of both composite and unreinforced samples prior to and immediately following tensile straining. Tension tests were conducted to various strains as well as to fracture and an extensometer was employed to obtain accurate measurement of the axial strain. The MMC material exhibited a continuously increasing dilatation during tensile straining while the unreinforced 6061 control material deformed plastically at constant volume. Careful metallographic preparation revealed particle cracking in all MMC samples throughout the range of strains examined. A clear trend of increased frequency of particle cracking was observed. Void formation and growth due to cracking of the particles was analyzed and shown to correlate with the dilatation observed during tensile straining of the composite. Linkage of such voids is proposed as the mechanism of crack propagation at failure of the MMC.

TABLE OF CONTENTS

ACKNOWLEDGMENT

I would like to thank the Army Research Laboratory/Army Research Office for financial support of this research. I would also like to thank my advisor, Dr. Terry R. McNelley for his encouragement and guidance during the course of this thesis. His patience and enthusiasm made this research a far less onerous task. I would also like to thank Rich Hashimoto for his many hours of assistance with laboratory equipment. Finally, this project would not have been possible without the love and support of my wife Antonia. Thank you.

I. INTRODUCTION

Engineered materials are those that have had their properties modified during processing or fabrication in order to enhance desired characteristics and minimize undesirable attributes. The ability to tailor the properties of engineered materials to the requirements of potential applications has generated strong interest in utilizing them in a growing range of applications. Of particular interest here are the engineered materials known as particle-reinforced metal-matrix composites (MMCs).

In particle-reinforced MMCs, a metal constitutes the matrix in which the reinforcing ceramic particles are dispersed. The hard ceramic particles result in a material with specific characteristics that are intended to be are superior to those of the metal alone. Thus, the ceramic particles can provide enhanced stiffness and improved strength and wear resistance while the metallic matrix contributes ductility and toughness. In addition, the particulate nature of the reinforcement should result in a nearly isotropic material in contrast to the highly anisotropic character of continuously reinforced composites.

One limiting factor in the widespread application of composite materials is their generally higher cost. Initially, these materials were produced by powder metallurgy methods wherein ceramic and metal powders are blended together and then consolidated by application of pressure at elevated temperature. More recently, development of ingot metallurgy methods by DURALCAN-USA, of Novi, MI has led to the promise of higher volume, lower cost production of MMC's. These methods involve the introduction of the

reinforcing particles while the matrix metal is molten, with subsequent processing by conventional ingot metallurgy methods. [Ref. 1]

Although offering properties superior to those of monolithic materials in many ways, MMCs also have their drawbacks. Poor fracture toughness [Ref. 2] and low ductility compared to un-reinforced counterpart materials have also limited their acceptance and widespread use; these issues have been the focus of considerable research activity [Ref. 3]. At the NPS, thermomechanical processing (TMP) of aluminum alloys which have been reinforced either with Al_2O_3 and consolidated by ingot metallurgy methods, or by SiC and consolidated by powder metallurgy methods, has been studied extensively [Refs. 4-11]. In recent work, TMP methods designed to homogenize particle distributions while simultaneously refining the matrix grain structure have been shown to confer greatly improved ductility - strength combinations in ingot-processed 6061 Al containing either 10 or 20 volume percent of Al_2O_3 particles [Ref. 12]. More recent work has concentrated on detailed examination of particle redistribution during TMP and the microstructural mechanisms of the failure of these 6061 Al - Al_2O_3 MMCs during tensile deformation. Apparently, load is effectively transferred to the reinforcement particles during both elastic and plastic straining as reflected in cracking of reinforcement particles during the latter stages of deformation. Void growth then occurs in the matrix in regions surrounding the fractured particles with failure then occurring due to linkage of these voids across a transverse plane of the specimen [Ref. 1].

The present investigation seeks to investigate, in more detail, the deformation and failure of a 6061 Al - 20 volume percent Al_2O_3 MMC during tensile straining. The goal

of this research is to better understand the mechanisms governing ductility of this composite during tensile loading. Of particular interest is the investigation of particle cracking during tensile deformation and the manner in which this process leads to failure. The ultimate goal is to describe the mechanisms involved in the processes of load transfer, particle cracking and crack linkage in this material.

II. BACKGROUND

Before entering into a detailed discussion of the mechanical behavior and failure of MMC's, a brief discussion of composite materials and the methods by which they are evaluated is presented.

A. COMPOSITES AS ENGINEERED MATERIALS

The investigation of composite materials is not a new endeavor in engineering. Composites have been in use for thousands of years; the first adobe brick ever allowed to dry in the sun was, strictly speaking, an engineered composite material. Beaten straw provided the reinforcing fibers in the clay and mud mixture that acted as the matrix of this important structural material.

To be defined as such, a composite material must satisfy three basic criteria. First, a composite material is one that has been manufactured or fabricated in some manner, i.e. it is a man-made material. Secondly, the material must consist of two physically and/or chemically distinct and dissimilar phases, distributed in three dimensions such that there are separating interfaces between the phases. Finally, the combination must have characteristics distinct from those of the individual materials that it comprises.

Composite materials are generally classified in terms of the reinforcement method and the matrix material. Composites are most often reinforced either by continuous fibers

or by discontinuous whiskers or particles. Reinforcement by continuous fibers allows for the optimum load transfer when the continuous fibers are aligned in the direction of applied loads. The matrix generally contributes relatively little to the composite strength and the material tends to be highly anisotropic in character. In contrast, load is less effectively transferred to the reinforcement when the material is discontinuously reinforced by the addition of particles. However, the material may also exhibit nearly isotropic characteristics. In such particle reinforced materials, matrix strength is more critical to the overall strength of the composite [Ref. 13]. Figure 2.1 shows a schematic diagram of various reinforcement types, geometries, and orientations [Ref. 14].

The three main matrix-based classifications of composites are: Ceramic Matrix Composites (CMCs); Polymer Matrix Composites (PMCs); and Metal Matrix Composites (MMCs). In CMCs, continuous fibers are generally incorporated with the goal of improving the CMC toughness and to increase its ability to resist catastrophic failure [Ref. 15]. The matrix is an intrinsically strong and stiff material and provides the primary contribution to strength. Because the matrix and the reinforcement are brittle materials, toughening must rely on control of interfacial bond characteristics. The second class of composites, PMCs, represent the most widely utilized category of composite materials. Applications range from aerospace components to sporting goods. Many applications rely on the high stiffness- and strength-to-weight ratio attainable by the utilization of high-modulus fibers, e.g. graphite, in such materials. In such cases, the reinforcement provides increased stiffness and strength while the polymer matrix serves primarily to hold the reinforcing fibers in place and transmit applied loads to the fibers.

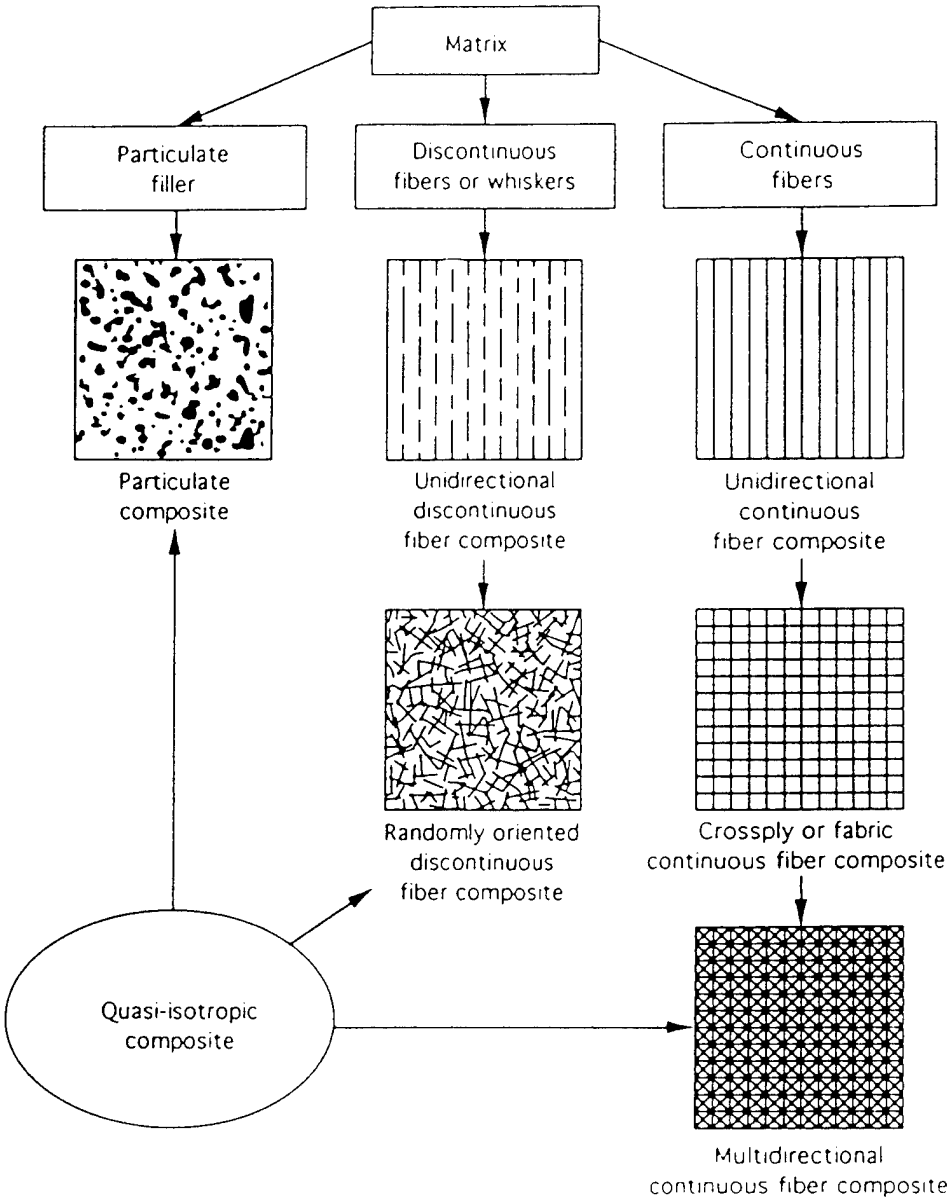

Figure 2.1 Classification of composite material system. From Reference [14].

Since the initial work on MMCs in the early 1950's, metal matrix composites have been the subject of intense scrutiny. Continuously reinforced MMC's also demonstrate high specific strength and stiffness, and also possess better high temperature capability than PMCs. In addition, MMC's generally offer greater thermal conductivity combined with good thermal shock resistance [Ref. 17]. Because of these characteristics, their value in high temperature applications has become increasingly apparent.

Discontinuously reinforced MMCs generally exhibit lower specific strength and stiffness than continuously reinforced materials but are more nearly isotropic in behavior. Discontinuously reinforced MMCs containing relatively low volume fractions of particles (e.g. 0.1) may offer improved stiffness but otherwise behave similarly to unreinforced metals. As volume fraction is increased, strength and stiffness is improved but often with unacceptable loss of ductility and toughness. The strength-temperature diagram in Figure 2.2 presents the performance regimes for several different groups of materials, including composites as well as other more traditional engineering materials. The excellent strength to weight ratios of MMCs' at elevated temperatures is clearly evident. [Ref. 16].

The production/fabrication methods of metal matrix composites has continued to evolve over the years. Powder metallurgy methods, originally developed in the 1950-60's [Ref. 18], are increasingly being supplemented by recent new developments in fabrication techniques. Spray forming, squeeze casting, high-pressure die casting and vacuum pressing are all methods that have been more recently developed and have yielded considerable success [Refs. 19-22]. Of particular interest in this research is the ingot metallurgy method recently developed by DURALCAN. It should be noted that

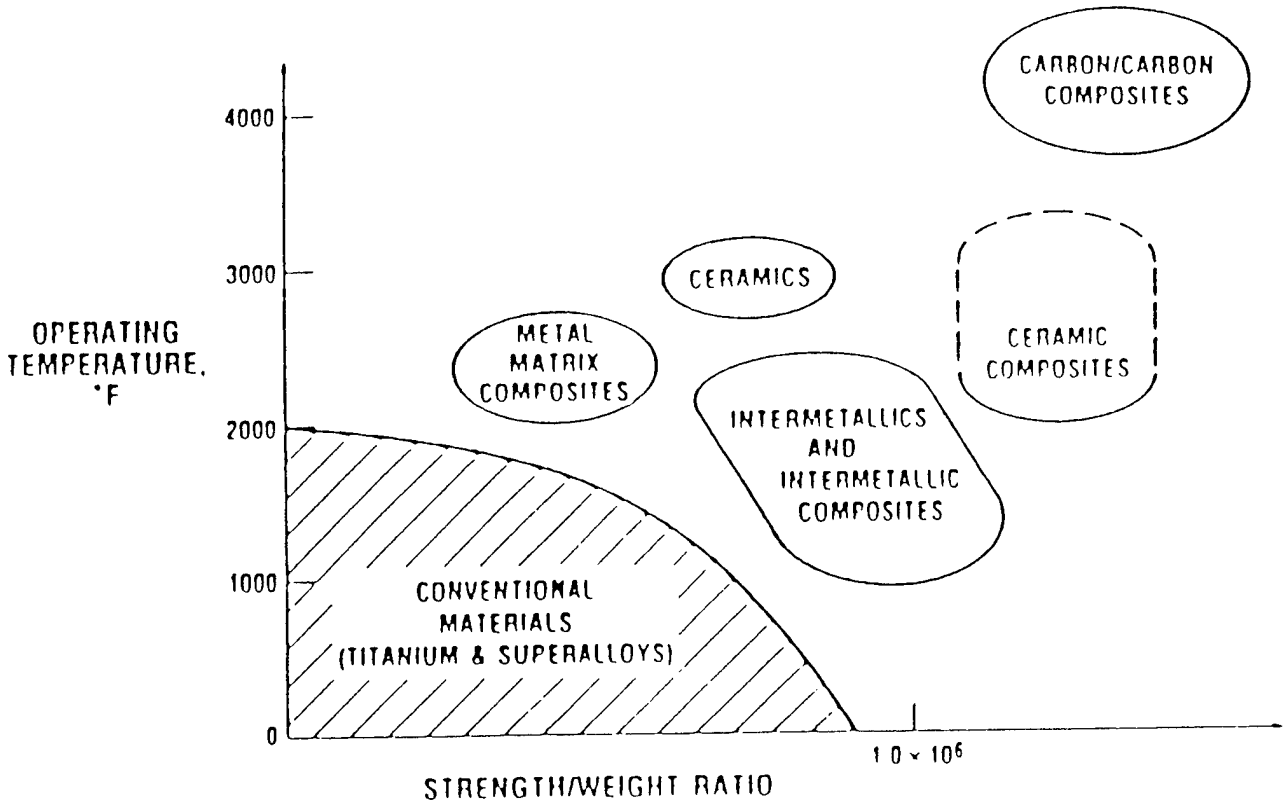

Figure 2.2 Performance map of various high temperature materials in terms of operating temperatures (°F) and strength/weight ratio. From Reference [15].

this procedure utilizes relatively large reinforcement particles: diameters are generally 10-30 μm as compared to 1-10μm in conjunction with powder metallurgy methods. Larger particles may be more readily dispersed in the matrix; strengthening requires load transfer to the dispersed particles by interfacial shear and so the matrix/particle interfacial characteristics are important to these MMCs [Ref. 23].

For engineering purposes a primary consideration in the development of discontinuously reinforced MMC's is the contribution of the particulate reinforcement to the composite elastic modulus. For example, by adding 20 volume percent of Al_2O_3 ($E_{Alumina}$ = 410GPa) particles to an aluminum alloy matrix (E_{Al} = 70GPa), we can produce a composite can be produced that retains a measure of the aluminum's ductility and toughness while attaining an elastic modulus of 110GPa, which is approximately 50% greater than that of the unreinforced matrix. The density of the composite is raised only slightly above that of unreinforced aluminum.

B. PERFORMANCE ASSESSMENT IN COMPOSITE MATERIALS

The Rule of Mixtures equations may be employed to predict the upper and lower bounds on the elastic modulus of a composite. [Ref. 23]. The upper bound corresponds to isostrain loading, while the lower bound corresponds to isostress loading. The isostrain and isostress states relate to the loading conditions for a unidirectional, continuously reinforced material as depicted Figure 2.3 [Ref. 23].

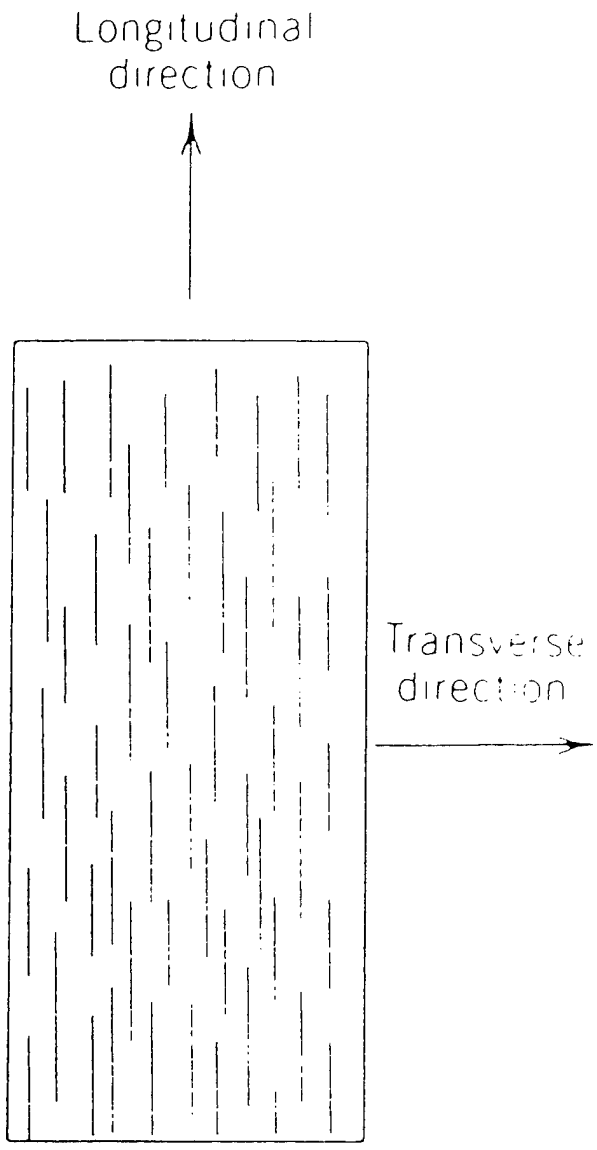

Figure 2.3 Direction of stress with regard to particle orientation. From Reference [23].

Under isostrain conditions the matrix and the reinforcement material experience identical strain. Such is the case in a fiber reinforced composite where the load is applied parallel to the axis of fiber orientation. This condition is taken as the upper bound for particle reinforced composites:

$$E_c = E_m V_m + E_p V_p \qquad (2.1)$$

where E = composite modulus elasticity, V = volume fraction and c, m, p represent the composite matrix and particulate phases.

The isostress condition is defined by loading in which both phases are subjected to the same stress. This is approximately true in the case of a unidirectional fiber reinforced material when the applied load is oriented 90 degrees off the axis of the fiber orientation. This transverse loading exposes both the matrix and the reinforcement to nominally the same stress. This situation provides a lower bound estimate for particulate reinforced composites:

$$E_c = \frac{E_m E_p}{V_m E_p + V_p E_m} \qquad (2.2)$$

Figure 2.4 [Ref. 23] shows a typical plot of composite elastic modulus versus volume percent of particles for Tungsten particle-reinforced Copper MMCs. It can be seen that all experimental data points fall within the region described by the upper and lower bound Rule of Mixtures equations. It is important to note that these two equations are based on the following assumptions:

1. the reinforcements (particles or fibers) are homogeneously distributed;

2. there is good load transfer at the interface between the reinforcements and the matrix, with no significant debonding; and

3. the reinforcements are defect free and unbroken.

Clearly, the presence of cracked particles would diminish the amount of load effectively transferred to the particles, causing the overall elastic modulus to decrease. Indeed, modulus measurement, e.g. by ultrasonic methods, may prove useful in evaluating the extent of particle damage in such MMCs.

Poisson's ratio is an additional coefficient that is important in describing both elastic and plastic response in materials. A metal generally deforms elastically at first and then plastically during tensile straining. While elastic deformation is completely recoverable because interatom bonds are only stretched, the plastic deformation is permanent because dislocation motion or other mechanisms of plastic deformation result in atoms changing nearest neighbors. In the case of deformation induced by uniaxial loading, the sample displays strain not only in the direction of the applied force but also along axes orthogonal to the applied stress. This results in a lateral contraction of the sample under tension. The relationship between the strain associated with the applied stress and its accompanying lateral strain during this uniaxial loading is given by Poisson's Ratio (ν):

$$\nu = -(\varepsilon_x/\varepsilon_z) = -(\varepsilon_y/\varepsilon_z) \qquad (2.3)$$

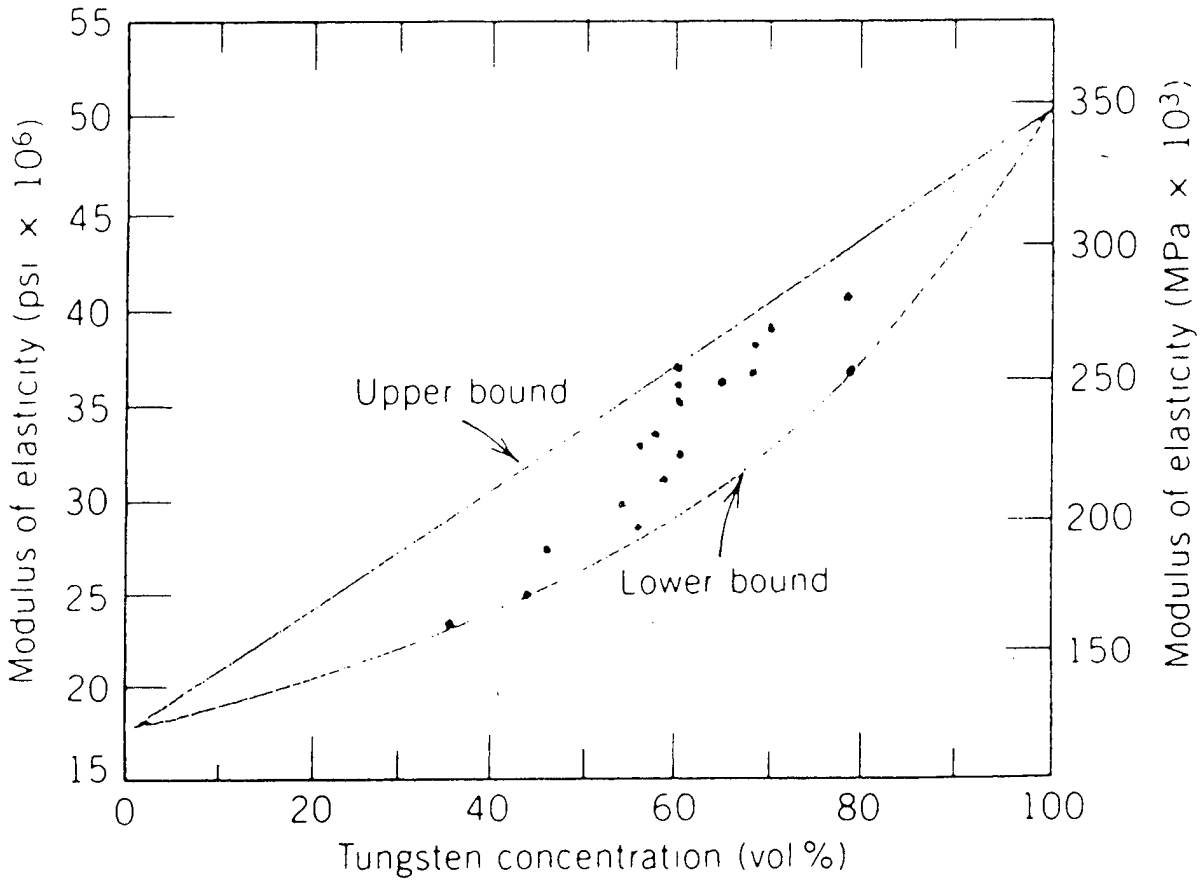

Figure 2.4 Modulus of elasticity versus volume percent tungsten for a composite of tungsten particles dispersed within a copper matrix. From Reference [23].

where ε_x and ε_y = principal strains along lateral axes (perpendicular to axis of applied force) and ε_z = principal strain in direction of applied force. Theoretically, a metal behaving in a perfectly plastic manner undergoes no net volume change and has a maximum value of $\nu = 0.5$. If one assumes that volume is constant, then the dilatation (the ratio of volumetric change to initial volume) must also be equal to zero:

$$\Delta V/V_0 = 0 \qquad (2.4)$$

where ΔV = change in volume, and V_0 is the original volume. By definition of the dilatation:

$$\Delta V/V_0 = \varepsilon_x + \varepsilon_y + \varepsilon_z \qquad (2.5)$$

where ε_z is the principal strain in direction of applied force and ε_x ,ε_y are the resultant principal strains perpendicular to tensile axes.

Using the definition of Poisson's ratio for the case of uniaxial loading, and assuming isotropic behavior, the following relationship can be stated:

$$\Delta V/ V_0 = \varepsilon_a + 2\varepsilon_l = \varepsilon_a(1-2\nu) = 0 \qquad (2.6)$$

Then $\nu = 0.5$, where ε_a is the strain in the axial direction, and ε_l is the strain in any lateral direction. In the event that void formation occurs during tensile extension, $\Delta V/ V_0 > O$, and $\nu < 0.5$. Separate measurements of ε_a and ε_l provide a ready method to evaluate such dilatational defects; and the dependence of E and ν may provide insight into the nature of the related processes.

Particle cracking is not considered to be the only possible cause of fracture and tensile failure in MMC's. Past research in the field of discontinuously reinforced MMCs has encompassed a wide variety of potential causes of material failure. These include: matrix failure, debonding at the particle-matrix interface, and mechanisms related to non-uniform distribution of particles, as well as particle cracking.

The various causes and initiators of debonding at the reinforcement/matrix interface have been the subject of significant research. For example, the superior stiffness, strength, and high temperature capability of SiC reinforced aluminum has long been overshadowed by its poor impact resistance and low toughness [Ref. 24]. Recent research has attempted to correct this problem by introducing microstructurally toughened composites [Ref. 25]. In this case, the SiC particles are surrounded by regions of aluminum matrix that are embedded with fine, cylindrical SiC 'pseudo fibers'. Through this technique superior "plastic behavior" of the composite material is achieved. This can be seen in Figure 2.5 [Ref. 24]. Recent literature has focused on the importance of successful wetting and bonding of particles to the matrix to improve fracture toughness[Refs. 25 - 26], while additional research has concentrated on the prevention of component diffusion through the interfacial boundary [Ref. 27].

Numerous studies have linked the mechanical properties of particle reinforced metal matrix composites to the uniformity of particle distribution [Ref. 1]. Research in this laboratory has shown that true processing strains on the order of 4.0 are required to achieve a homogenous distribution of particles in the case of alumina reinforced aluminum alloys [Ref. 12]. Further, it was found that while cold working was generally

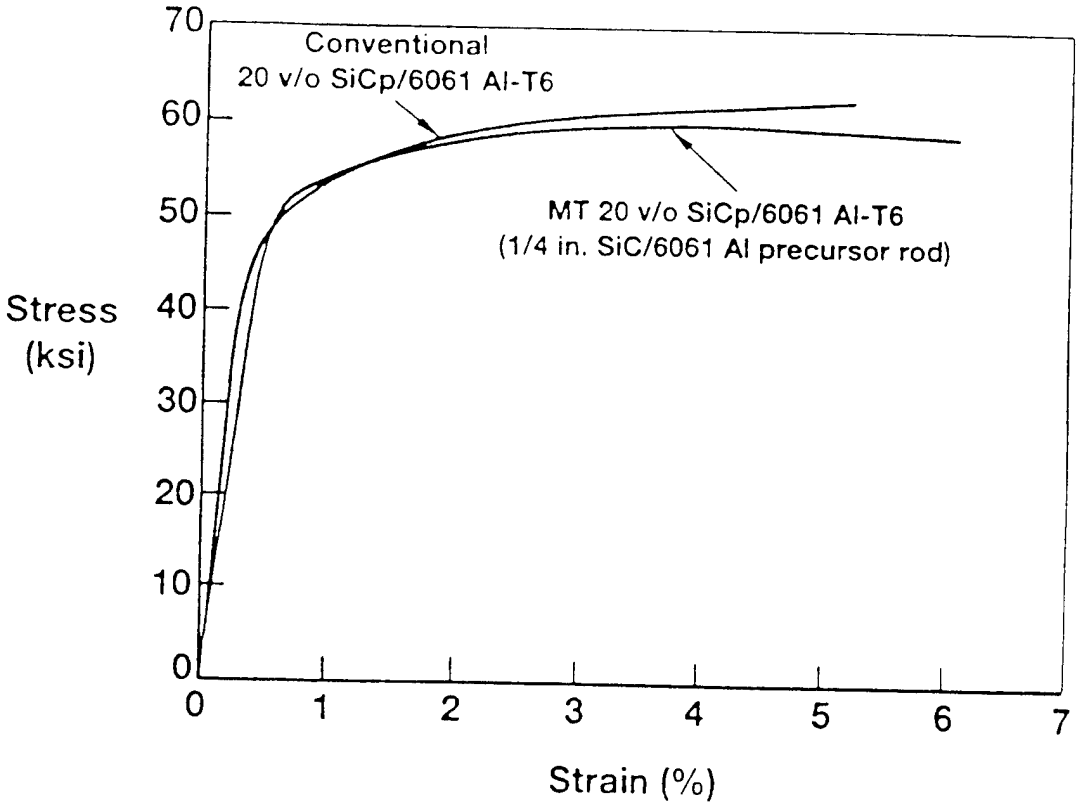

Figure 2.5 Plot of tensile properties of conventional and microstructurally toughened SiC/Al. From Reference [24].

less effective, hot processing effectively redistributed the ceramic particles by grain boundary sliding following recrystallization in particle clusters [Ref. 1]. This resultant homogenous particle distribution achieved through theromomechanical processing led to an increase in both tensile ductility [Ref. 6], and improved fracture resistance of the composite [Ref. 2]. The relationship between homogenous particle distribution and particle cracking in a SiC reinforced aluminum alloy has been recently investigated by Lloyd and others [Ref. 29-30]. This work indicated that particle fracture initiates in regions of clustered or banded particles that arise during fabrication. It was also observed that particle cracking occurred not only at the fracture site but at various locations along the gage length. Recent research has found that particle size and degree of strain experienced were identified as factors controlling particle cracking [Ref. 31]. This research indicated that a higher number fraction of particles cracked in composites reinforced with large particles and with high matrix yield strengths. These results were supported by Singh and Lewandowski in their study of SiC-reinforced aluminum alloys [Ref. 32]. Particle cracking was found to increase linearly with matrix strain. In addition, their research concluded that the Poisson's Ratio in elastic behavior of the composites was significantly lower than for the unreinforced alloy. They concluded that this change in Poisson's Ratio was dependent on both failure of the matrix and particle cracking with increasing strain. It was proposed that the higher elastic modulus and lower Poisson's Ratio of the ceramic reinforcement is a significant cause of this particle fracture.

Work at in this laboratory would seem to lend support to this position. Research by Ballou [Ref. 1] found that in Al_2O_3 reinforced aluminum alloys, tensile failure resulted from particle cracking followed by the formation of voids at cracked particles through ductile tearing in the matrix. Clearly, particle cracking is not simply a by-product of material fracture but is critically involved in fracture initiation and material failure.

This research will attempt to shed further light on the role of particle cracking in the failure of a selected MMC.

III. EXPERIMENTAL PROCEDURE

A. MATERIAL

The composite material examined in this work was a particle-reinforced 6061 Al - 20 volume percent Al_2O_3 metal matrix composite produced by DURALCAN - USA, currently located in Novi, MI. The material was produced via a proprietary ingot-metallurgy method developed by DURALCAN [Ref. 1]. The chemical composition of the 6061 Al - 20 volume percent Al_2O_3 matrix alloy was provided by the manufacturer (in weight percent) is listed in Table 3.1:

Table 3.1 Composition of 6061 Al - 20 Volume Percent Al_2O_3. From Reference [4].

Si	Fe	Cu	Mn	Mg	Cr	Zn	Ti	Al
0.55	0.05	0.27	<0.01	1.00	0.12	0.01	0.01	Remainder

Unreinforced 6061 Al-T6 material was obtained from NPS stock. The 12.5 mm (0.5 inch) diameter cylindrical bar stock was used to machine tensile samples for control purposes during the mechanical testing portion of this research. This material had the composition listed in Table 3.2 [Ref. 35]:

Table 3.2 Composite of 6061 Aluminum. From Reference [35].

Si	Mn	Mg	Cr	Al
0.6	0.28	1.00	0.20	Remainder

B. PROCESSING HISTORY

Details of the thermomechanical processing schedule utilized with the MMC examined in this research were provided by Ballou [Ref. 1]. The schedule is shown schematically in Figure 3.1 and is briefly summarized below.

The composite was consolidated by direct chill casting in the form of a 17.8 cm (7.0 inch) diameter billet which was sectioned into lengths of about 51 cm (20 inches) by the manufacturer. All extrusions were conducted by Universal Alloy Inc. of Anaheim, CA. The first extrusion was done at 440°C to produced a bar of 6.3 cm (2.5 inch) diameter. The bar was sectioned to provide billets which were extruded again at 440°C to a diameter of 16.3 mm (0.642 inch). The extrusion process was followed by two separate cold draw/anneal cycles, with the anneals both conducted at 350 °C. The final draw/anneal cycle reduced the MMC to its final diameter of 12.5 mm (0.5 inch). The resulting total true strain experienced by the composite in the received state was 5.32.

This amount of strain level was found in previous work by Ballou and Longenecker [Refs.1&2] to provide a uniform and homogeneous composite microstructure by redistribution of the reinforcement particles and refinement of the matrix microstructure.

C. TENSILE SAMPLE FABRICATION

Button-head tensile specimens of the MMC as well as the unreinforced 6061-Al alloy were machined from 12.5 mm (0.5 inch) diameter bars of the respective materials to

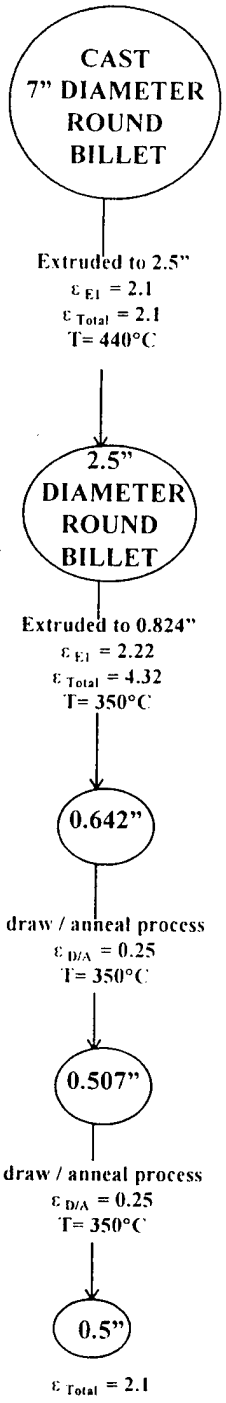

Figure 3.1 Processing schedule for the Al 6061-20 volume percent Al_2O_3 metal matrix composite. Size dimensions and strains are listed for each step.

the dimensions specified in Figure 3.2. The composite material was found to be highly abrasive and all cutting and machining had to be accomplished utilizing diamond and cobalt cutting and milling tools. The buttonhead sample design used in this work was intended to provide a gage length at least five times the gage diameter. Also, the shank diameter was designed to ensure that plastic deformation in the grip end sections of the sample could not occur prior to fracture in the gage length.

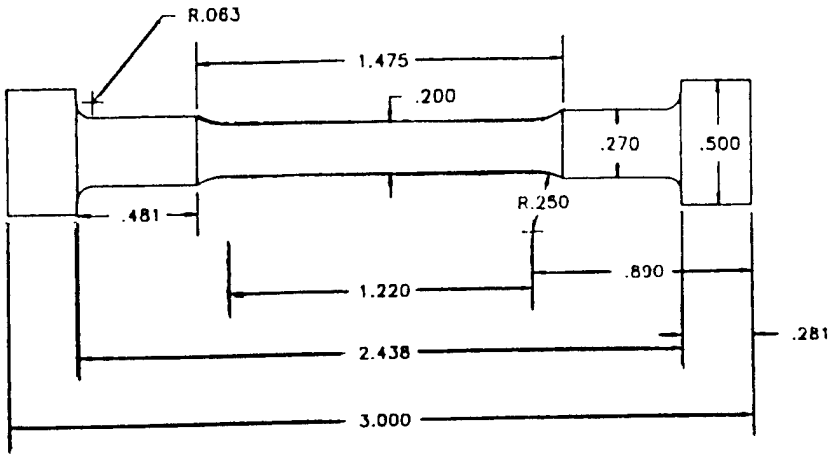

Figure 3.2 Tensile Test Button-head design. These samples were machined from 0.5" (12.77mm) diameter extruded bars.

D. HEAT TREATMENT

A total of eight button-head samples were machined from as-received MMC material and all were heat treated identically. Oven temperatures were monitored by K-type thermocouples attached to an OMEGA Model HH21 Microprocessor Thermometer. Each sample was solutionized in a Lindberg Type 51222 furnace at 545 °C for 70 minutes. Solutionized samples were immediately quenched into still, ambient-temperature water and placed into a Lindberg Blue-M oven, Model OV-490A-3, set at 160 °C for aging. This is the recommended aging temperature for 6061 Al [Ref. 33] and

has been utilized in previous work, e.g. by Schaeffer [Ref. 8] and Eastwood [Ref. 11]. The samples were aged for 18 hours and then allowed to air-cool and equilibrate at room temperature prior to mechanical testing.

E. TENSION TESTING

1. Diametral Measurements (Before Testing)

After the samples had cooled to room temperature, diametral measurements of their gage sections were made. Measurements were made using a Mitutoyo Analog Micrometer with a rated precision of 0.0001 inches. Five equally spaced points along the gage length of each test sample were selected. The diameter at each point was measured three times, with a 120° rotation about the longitudinal axis between each measurement. This allowed for any ellipticity of the sample to be taken into account. The diameter at the midpoint at the gage length of the sample was measured first. Two points located 6.2 mm (0.24 inch) on either side of the center point were then measured and finally points 12.4 mm (0.44 inch) were measured. Four 6061 Al tensile samples were diametrally measured in an identical manner.

2. Diametral Measurements (After Tension Tests)

After tension testing was completed, the measurement process was repeated. In this case, the incremental distance between subsequent measurement points was altered to correspond to 20% of the measured gage length of the sample in order to account for sample extension. By this process, 15 diametral measurements were obtained for each of the eight composite samples as well as the four Al 6061 samples. These diametral measurements were analyzed by the Student t-test to assess the statistical validity of the resulting strain data. [Ref. 34]

For each set of 15 diametral measurements the mean diameter (X_{mean}) was determined. The standard equation for mean determination was used:

$$X_{mean} = \frac{X_1 + X_2 + \ldots X_N}{N} \quad (3.1)$$

where X_N is each individual measured diameter and N is the total number of measurements.

The standard deviation (S_N) for each set of data was also calculated:

$$S_N = \frac{\left((X_{mean} - X_1)^2 + (X_{mean} - X_2)^2 + \ldots (Xmean - X_N) \right)^{1/2}}{(N-1)} \quad (3.2)$$

Once the standard deviation had been calculated for all measurement sets, the largest value obtained was selected for use in the confidence interval determination. See Table 3.3 for tabulated mean average and standard deviation results. Due to the importance of accurate diametral measurements to subsequent diametral strain determinations, a 99% confidence interval was deemed necessary. From a standard t-test table [Ref. 34], the t-value for a 99% confidence interval ($t_{0.005}$) was determined. The following equation was used for precision interval (p_N) determination:

$$p_N = \frac{\pm (t_{0.005})(S_N)}{(N)^{0.5}} \quad (3.3)$$

F. THE MECHANICAL TESTS

Tension tests were conducted on eight separate composite samples as well as four samples of the reference 6061 Aluminum material. Tensile test data was obtained from an Instron computer-controlled Model 4705 Mechanical Testing Machine. Plots of

engineering stress versus engineering strain were obtained from the Instron SERIES IX Material Testing System software. All tension tests utilized a constant crosshead speed of 0.2 mm/min and were conducted at room temperature (20-25^{0}C). An Instron Model 2620-824 Extensometer was employed to monitor and measure axial strain during tensile extension. The test data acquisition rate was five points per second and the data were then backed up on 3.5" floppy diskettes. All of the composite samples were pulled to strains in the plastic range of the stress-strain curve and two were pulled until failure. The unreinforced 6061 samples were pulled to plastic strains in a range corresponding to the ductility of the composite. The computer program reports provided additional data on yield strength and modulus of elasticity as well as total strain.

G. DATA CONVERSION

Data was converted and exported from the Instron compressed file format into ASCII files for use in Microsoft Excel. The raw data could then be edited and structured as needed.

H. METALLOGRAPHIC SAMPLE PREPARATION

The schedule provided in Table 3.4 was used for grinding and polishing in the preparation of the composite specimens selected for metallographic analysis. The schedule was obtained from the Buehler Corporation and has been successfully utilized in

previous work (Refs.1-3). All grinding was accomplished on a Struers Knuth-Rotor 3, while polishing was conducted on a Buehler Ecomet 3 Variable Speed Grinder/Polisher.

I. OPTICAL MICROSCOPY

In order to evaluate the role of particle fracture during plastic deformation prepared samples of the composite material were examined in a Zeiss ICM-405 Optical Microscope. After the samples had been prepared and examined visually, 35 mm photographs were taken using Kodak TMX 100 black and white film and a Nikon 35 mm SLR camera (utilizing the Zeiss Photographic Microscope with a vertical eyepiece adapter).

J. SCANNING ELECTRON MICROSCOPE IMAGING

All SEM fractography analysis was conducted utilizing a Model S-200 Cambridge Scanning Electron Microscope at the Naval Postgraduate School.

PRE-TENSILE TEST MEASUREMENTS			
Sample #	**Number of Measurements**	**Mean diameter (in)**	**Standard Deviation**
1	15	0.1998	8.0178×10^{-5}
2	15	0.1998	2.1712×10^{-4}
3	15	0.1996	1.8708×10^{-4}
4	15	0.1999	1.1650×10^{-4}
5	15	0.1999	1.8516×10^{-4}
6	15	0.1999	1.2248×10^{-4}
7	15	0.2000	1.0000×10^{-4}
8	15	0.1998	1.1339×10^{-4}

POST-TENSILE TEST MEASUREMENTS				
Sample #	**Axial Plastic Strain**	**Number of Measurements**	**Mean diameter (in)**	**Standard Deviation**
1	0.0076	15	0.1979	2.414×10^{-4}
2	0.0105	15	0.1989	1.2818×10^{-4}
3	0.0135	15	0.1983	1.3762×10^{-4}
4	0.0164	15	0.1983	1.1439×10^{-4}
5	0.0217	15	0.1976	2.480×10^{-4}
6	0.0250	15	0.1973	1.1738×10^{-4}
7	0.0322	15	0.1988	1.4722×10^{-4}
8	0.0398	15	0.1991	1.0343×10^{-4}

TABLE 3.3 Diametral Mean Averages And Standard Deviations.

Step Number	**Polishing Medium**	**Grit Size**	**Grit Diam. (microns)**	**Time (min)**	**Wheel RPM**	**Comments**
1	Carbide Paper	230	46	0.5	12" diam 300 RPM	1-5 lbf*
2	Carbide Paper	400	30	0.5	12" diam 300 RPM	1-3 lbf*
3	Carbide Paper	1000	18	2	12" diam 300 RPM	1-3 lbf*
4	Carbide Paper	2400	10	3	12" diam 250 RPM	1-3 lbf*
5	Carbide Paper	4000	5	3	12" diam 250	1-3 lbf*
6	diamond spray w/Metadi extender chemomet cloth		6	6-9	12" diam Slow spd	1-3 lbf*
7	diamond spray w/Metadi extender chemomet cloth		1	6-9	12" diam 300 RPM	1-2 lbf*
8	diamond spray w/Metadi extender micro cloth		0.05	1	12" diam 300 RPM	1-2 lbf*

Table 3.4 Specimen Polishing Abrasive Schedule.

IV. RESULTS AND DISCUSSION

The role of particle cracking during deformation and fracture of a 6061 Al-20 volume percent Al_2O_3 metal matrix composite was investigated by conducting tensile tests, each to a pre-determined strain. Dilatation was evaluated by careful measurement of both axial and diametral strains. Metallographic examination was employed to correlate dilatation data with microscopy.

A. MECHANICAL TESTING

The results from the tensile tests conducted on the eight samples of 6061 Al-20 volume percent Al_2O_3 and the four samples of 6061 Al are summarized in Table 4.1. Instron analysis programs produced displacement and total axial strain data for each sample. Plastic strain values were determined by subtracting the elastic strain corresponding to the applied stress at the cessation of straining (or fracture). This elastic strain was determined by extrapolating the elastic portion of the stress-strain curve to the stress in question; the elastic strain was determined for this stress and subtracted from the total strain.

The eight composite samples were pulled to various strains, including failure. Four aluminum samples were also tested over a similar range of strain values for comparison purposes. Axial strain values were based on extensometer data. Post-tensile-test diametral measurements resulted in the determination of corresponding diametral

6061 Al-20 Volume Percent Al_2O_3				
Sample #	Axial Plastic Strain	Diametral Strain	Volumetric Dilatation	Poisson's Ratio
	0	0	0	0
1	0.0076	-0.0035	0.0006	0.46
2	0.0105	-0.0045	0.0015	0.43
3	0.0135	-0.006	0.0015	0.44
4	0.0164	-0.0065	0.0034	0.40
5	0.0217	-0.009	0.0039	0.42
6	0.025	-0.008	0.0093	0.32
7*	0.0322	-0.0095	0.0132	0.29
8*	0.0398	-0.011	0.0187	0.26
6061 Al				
Sample #	Axial Plastic Strain	Diametral Strain	Volumetric Dilatation	Poisson's Ratio
	0	0	0	0
1	0.0157	-0.0075	0.0006	0.48
2	0.0255	-0.0125	0.00045	0.49
3	0.0356	-0.0175	0.00058	0.49
4*	0.0539	-0.0267	0.0005	0.50

Table 4.1 Summary of observed mechanical behavior (* indicates sample fracture).

strain values for each sample. Dilatation computations were conducted in accordance with Equation 2.6.

The dilatation values determined from the axial and diametral strain measurements and reported in Table 4.1 are plotted versus axial plastic strain in Figure 4.1 for both the composite and unreinforced control 6061 material. The composite exhibits dilatation from the onset of straining and the rate of increase of dilatation with strain appears to accelerate as the axial strain increases. In contrast, the unreinforced 6061 control material exhibits almost no dilatation during plastic deformation, as expected for plastic deformation of an ordinary metal. It is noteworthy that the dilatation

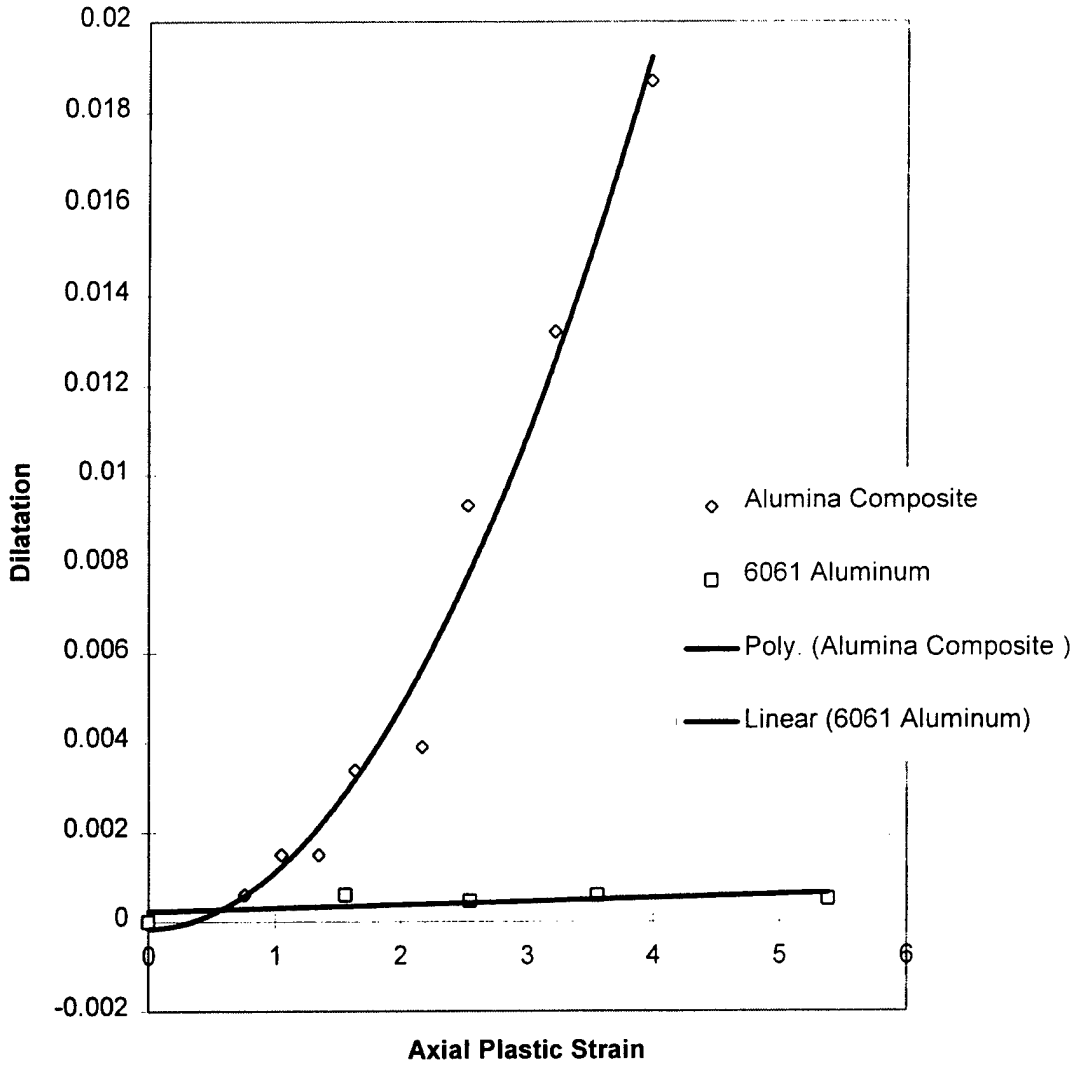

Figure 4.1 Plot of Dilatation versus Axial Plastic Strain for 6061 Al-20 volume percent Al_2O_3 and 6061 Al tensile samples

of the composite reaches a value 0.01 at an axial strain of about 0.025; this suggests that an appreciable portion of the apparent plastic deformation of the composite at this point is actually due to internal void formation.

Poisson's Ratio can be calculated from the axial and diametral strains and these data are included in Table 4.1 for both the composite and unreinforced 6061. In Figure 4.2 the calculated Poisson ratio, ν, is plotted versus apparent axial strain and it is seen that $\nu = 0.5$ for the unreinforced matrix alloy. In contrast, ν is strain dependent for the composite over the strain range investigated and decreases to a value of about 0.25 at an apparent axial strain of 0.04. This value is below the value of Poisson's Ratio for elastic behavior of the unreinforced matrix.

The dilatation of the composite material can be explained by a mechanism of particle cracking followed by internal void formation as particle fragments move apart during straining. Linkage of such voids would lead ultimately to fracture [Ref. 1]. It has been observed that both fractured and undamaged particles are present in 6061 Al-20 volume percent Al_2O_3 material prior to tensile loading [Refs. 1-2]. During tensile straining, load is increasingly transferred to the discontinuous particles within the matrix. These particles fail by cracking upon reaching their elastic limit. Once these particles fracture, voids start to form between the particle fragments. Initially limited by the diameter of the particle, these voids later expand outward, both axially and diametrally. Figure 4.3 from Ref. 1, shows a schematic representation of this process. Void growth continues until voids begin to link together forming an incipient crack.

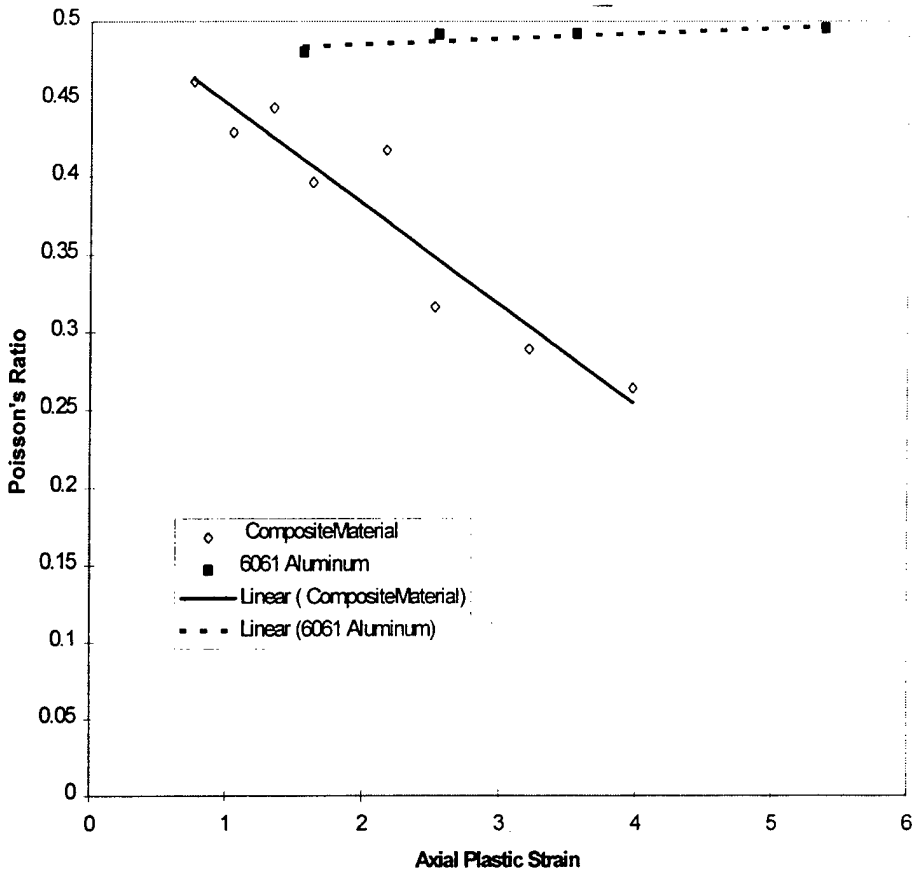

Figure 4.2 Plot of Poisson's Ratio versus axial plastic strain for 6061 Al-20 volume percent Al_2O_3 and 6061 Al tensile samples.

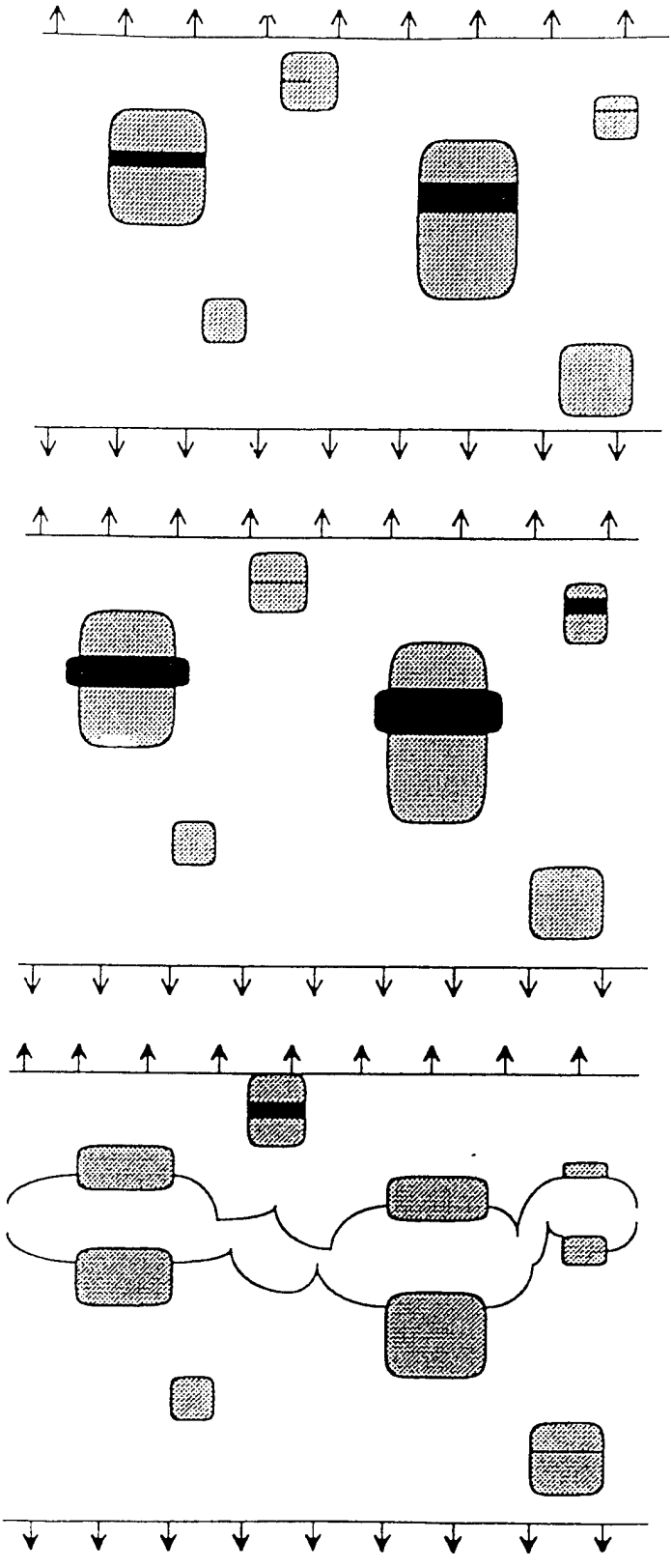

Figure 4.3 Schematic of the failure mechanism in this metal matrix composite. From Reference [1].

The mechanical data of the present work support such a mechanism of progressive cracking of particles, followed by void growth and coalescence. For this composite the observed dilatation increases with strain from the onset of plastic deformation. It is therefore reasonable to assume that continued straining of the sample results in both the formation of newly sundered particles and a greater separation in already broken particles. Together, these phenomena would create a progressive increase in void volume within the material. Such a mechanism would account for sample elongation during axial straining without diametral contraction.

B. MICROSTRUCTURAL EVALUATION

The foregoing suggests a simple relationship between the observed dilatation and the local processes of particle cracking in the composite. This is illustrated in the schematic of Figure 4.4.

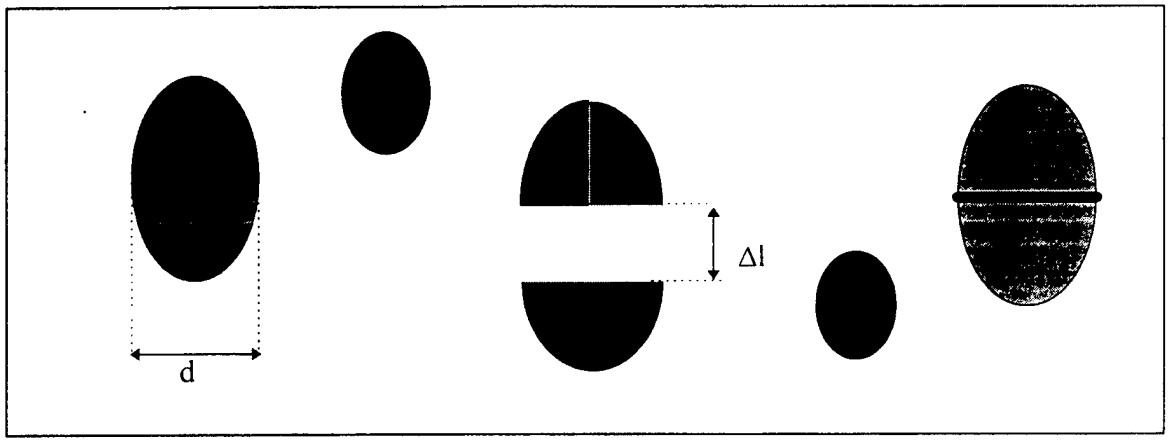

Figure 4.4 Schematic of particle cracking process.

The total number of particles per unit volume in the composite, N_T, is given by

$$N_T = \frac{V_f}{(4\pi/3)\,(dp/2)^3} \qquad (4.1)$$

where V_f is the volume fraction of particles of diameter d_p. The number of cracked particles per unit volume, N_c, is just

$$N_C = n_C N_T \qquad (4.2)$$

where n_C is the measured fraction of cracked particles. For each cracked particle there is an associated local dilatation, Δv, given by

$$\Delta v = (\Delta l_{sep})(\pi/4)(d_p)^3 \qquad (4.3)$$

where Δl_{sep} is the separation distance between particle fragments(Figure 4.4). These relationships may be combined to obtain the dilatation $\Delta V/V_0$ for the composite as

$$\Delta V/V_0 = N_c \Delta V = 3\, V_f n_C \Delta V_{sep}/2d_p \qquad (4.4)$$

where all terms have been defined. This relationship indicates that measurement of the fraction of cracked particles, n_C, and the mean separation distance, Δl_{sep}, by metallographic examination of deformed samples should allow direct correlation of the measured dilatation with the microscopic processes involved.

Metallographic preparation of four of the deformed composite samples was conducted according to the procedure outlined in the previous chapter. Photomicrographs of each of the four strained conditions of the composite material were analyzed quantitatively to obtain n_C. At least one thousand particles were examined as the sample base for this procedure. In each case, the total number of particles N_T and the number of

cracked particles, N_C, were determined for each of the four samples in order to calculate n_C. Figures 4.5(a) - 4.5(d) show typical microstructures of these samples subject to varying degrees of strain. Results of this analysis are summarized in Table 4.2. A plot of fraction of cracked particles versus axial plastic strain is shown in Figure 4.6. The unstrained material exhibited a significant fraction, n_C = 0.0324, or 3.24%, of cracked particles. This fraction then increased with strain and reached a value of 0.0947 in the fractured sample. It should be noted that this fraction was obtained from examination of regions remote from the fracture itself. The Scanning Electron Microscope (SEM) data from the fracture surface as well as direct observation of the crack profile suggest that virtually all particles are cracked at this location. SEM images of the fractured surfaces of both the composite material and the unreinforced 6061 Al alloy are provided in Figures 4.7(a) and 4.7(b). Measurement of Δl_{sep} values from micrographs was attempted and an increase in Δl_{sep} with strain was noted. However, in deformed samples it was not possible to determine whether fractured particles had failed due to prior processing or as a result of tensile deformation. For this reason, no attempt was made to determine the relationship between Δl_{sep} and ε_{axial}.

C. DISCUSSION

The results of this study appear to support the notion of a progressive particle cracking process during deformation of this material. Ambient temperature tensile strain measurements of the composite material demonstrated that the sample volume does not remain constant during tensile deformation. Instead, dilatation occurs progressively; this

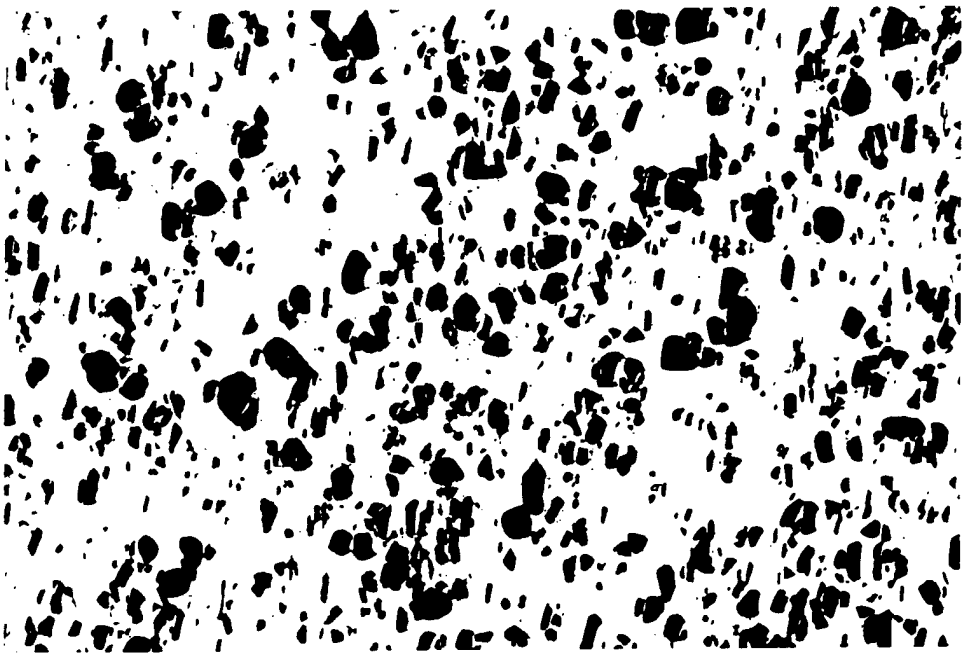

Figure 4.5(a) Optical micrograph of the 6061 Al-20 volume percent Al_2O_3 MMC which has undergone no tensile deformation.

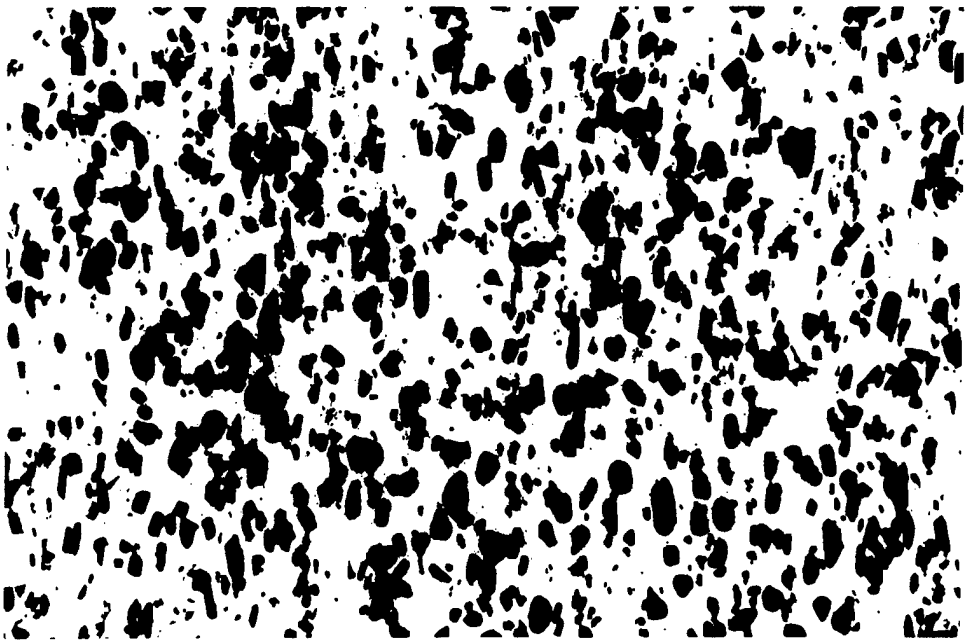

Figure 4.5(b) Optical micrograph of the 6061 Al-20 volume percent Al_2O_3 MMC which has been deformed in tension to an axial plastic strain of 0.0135. Tensile direction is vertical.

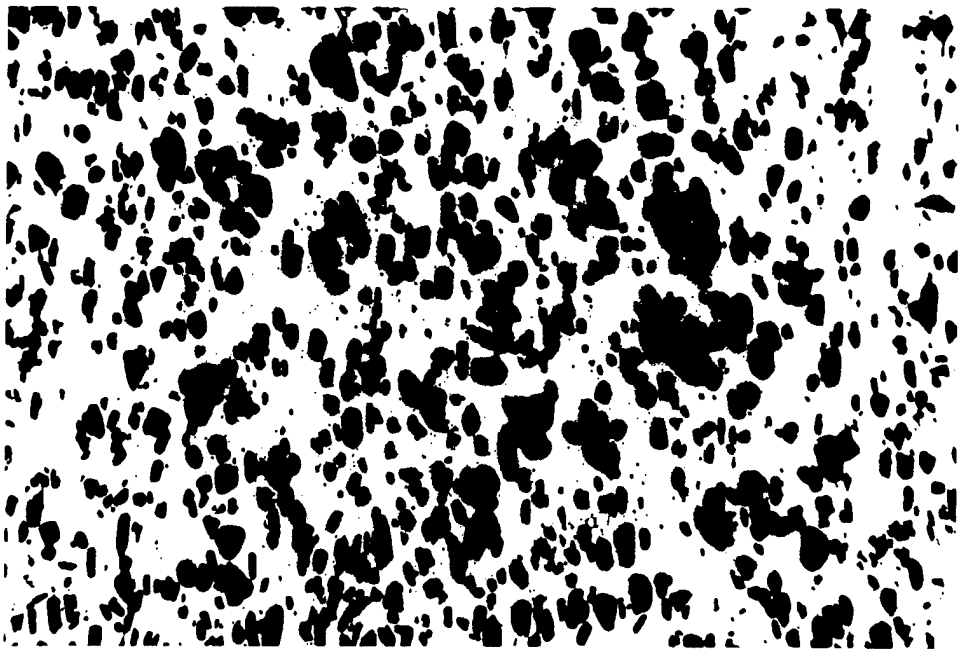

Figure 4.5(c) Optical micrograph of the 6061 Al-20 volume percent Al_2O_3 MMC which has been deformed in tension to an axial plastic strain of 0.0253. Tensile direction is vertical.

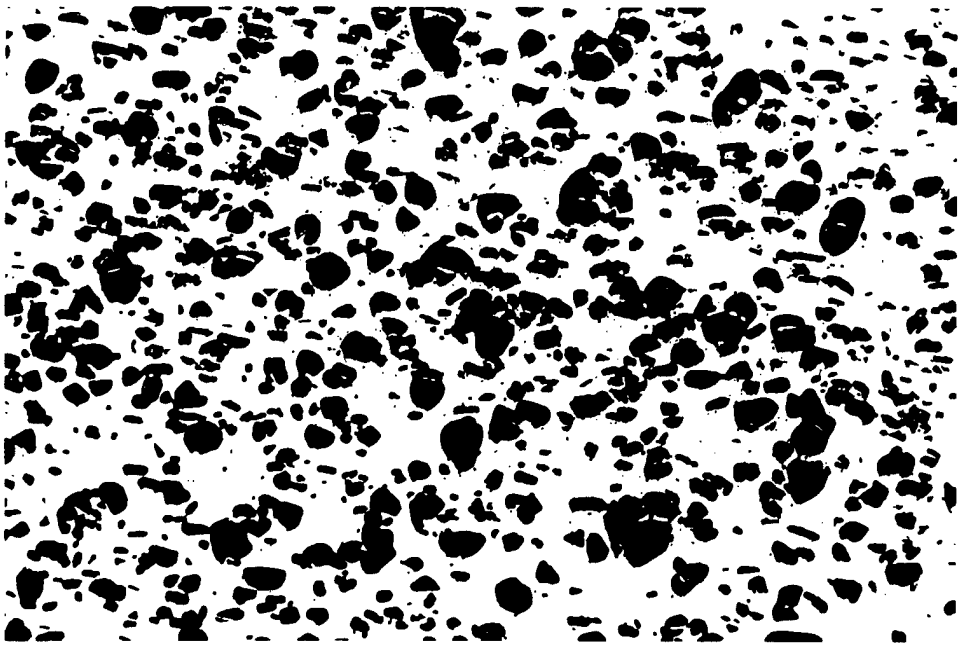

Figure 4.5(d) Optical micrograph of the 6061 Al-20 volume percent Al_2O_3 MMC which has been deformed in tension to an axial plastic strain of 0.0398. Tensile direction is vertical.

Table 4.2 Axial strain values with this corresponding fraction of cracked particles for 6061 Al-20 volume percent Al_2O_3 matrix.

Photos	Axial Strain	n_C
#1	0.0	0.0324
#2	0.0135	0.0447
#3	0.0253	0.09216
#4	0.0398	0.0947

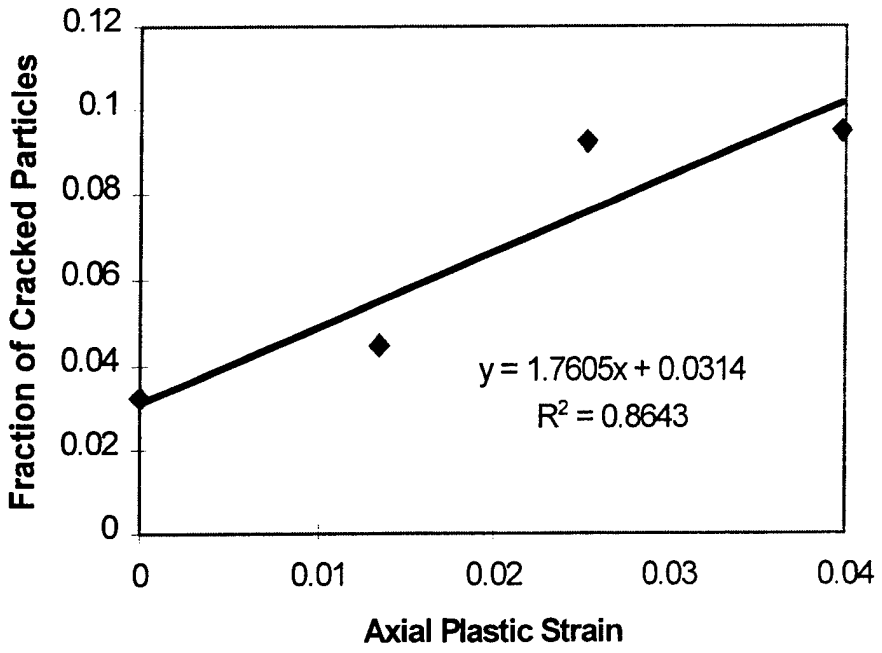

Figure 4.6 Plot of fraction of cracked particles versus axial plastic strain for 6061 Al-20 volume percent Al_2O_3 matrix.

concept of volume expansion is reinforced by the apparent linear dependence of the Poisson's ratio value on axial strain. The negative slope of ν versus ε_{axial} is consistent with the strain dependence of the dilatation. These observations suggest that the observed dilatation increases due to an increasing number of internal voids that form as particles crack in a successive manner during tensile deformation.

Optical microscopy provided further evidence of the role of particle cracking in the deformation and fracture behavior of the 6061 Al-20 volume percent material. It was observed that void formation occurred exclusively at fragmented particles. In addition, a calculation of the fraction of cracked particles revealed that the number of broken particles increased linearly as axial strain was increased.

These observations can be most easily be explained by a particle cracking process that is progressive, and that is dependent on the local stresses surrounding the reinforcement particles.

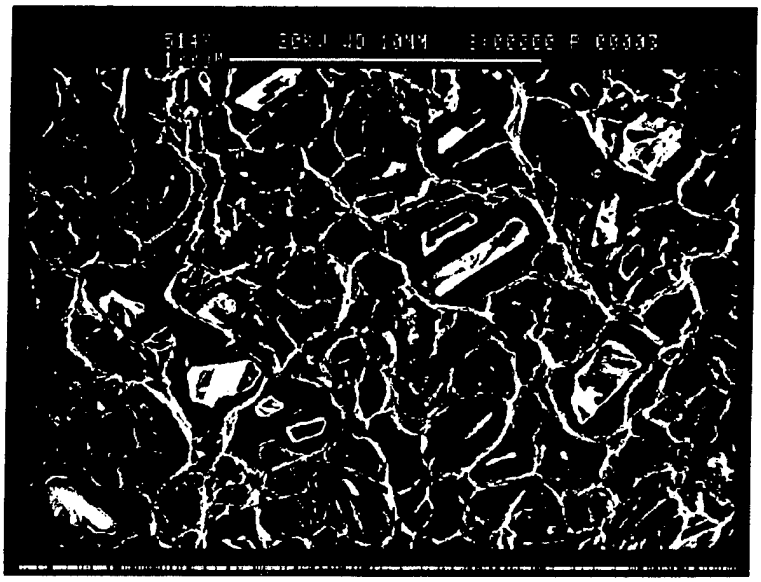

Figure 4.7(a) SEM micrograph for fracture surface of 6061 Al-20 volume percent Al_2O_3 MMC. Notice numerous faceted and cracked particles.

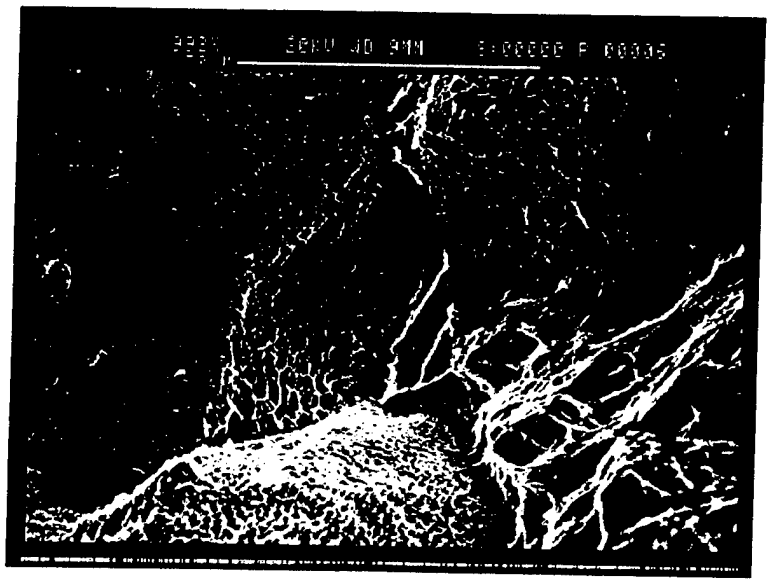

Figure 4.7(b) SEM micrograph of 6061 Al unreinforced sample. Surface indicates failure through microvoid formation followed by coalescence and ductile tearing.

V. SUMMARY

A. CONCLUSIONS

The following conclusions are drawn from this work:

1. The 6061 Al - 20 volume percent Al_2O_3composite demonstrated an increasing degree of dilatation as the axial strain increased.

2. The 6061 Al unreinforced alloy showed negligible dilatation. Inclusions in the material may account for the slight effect observed.

3. Void formation in the composite material occurred exclusively in association with fracture of particles.

4. The fraction of cracked particles in the composite material increased with the amount of axial strain.

5. Effective measurement of the average particle separation distance between cracked particle fragments is limited due to the uncertainty regarding the strain at crack initiation.

B. RECOMMENDATIONS

The following is a list of recommendations for further study.

1. Attempt to model the particle fracture and load transfer processes: a Finite Element Method (FEM) of analysis may prove useful in this effort.

2. Conduct a dilatation analysis for the 6061 Al - Al_2O_3 metal matrix composite for varying reinforcement volume fractions and a range of thermomechanical processing histories.

3. Conduct a local strain analysis through the measurement of particle separation distance in processed and unprocessed samples of the composite material.

LIST OF REFERENCES

1. Ballou, M.A., *The Effect of Thermomechanical Processing on the Tensile Properties and Microstructure of a 6061 Al- Al_2O_3 Metal Matrix Composite,* Master's Thesis, Naval Postgraduate School, Monterey, California, December 1995.

2. Quiles, F.N., *An Investigation of the Effects of Secondary Processing on the Fracture Properties of a SiCp-6XXX Al Composite,* Master's Thesis, Naval Postgraduate School, Monterey, California, June 1996.

3. Manoharan, M. and Lewandowski, J.J., "Crack Initiation and Growth Toughness of an Aluminum Metal-Matrix Composite", *Acta Metallurgica et Materialia*, Vol. 38, No. 3, pp. 489-496, (1990).

4. Hoyt, W. F., *The Effect of Thermomechanical Processing on Mechanical Properties of a Cast 6061 Aluminum Metal Matrix Composite,* Master's Thesis, Naval Postgraduate School, Monterey, California, December 1993.

5. Kalu, P.N. and McNelley, T.R., "Microstructural Refinement by Thermomechanical Treatment of a Cast and Extruded Al_2O_3 Composite", *Scripta Metallurgica et Materialia,* Pergamon Press, Vol. 25, pp. 853-858, (1991).

6. McNelley, T.R. and Kalu, P.N., "The Effects of Thermomechanical Processing on the Ambient Temperature Properties and Aging Response of a 6061 Al- Al_2O_3 Composite", *Scripta Metallurgica et Materialia,* Pergamon Press, Vol. 25, pp. 1041-1046, (1991).

7. McNelley, T.R. and Kalu, P.N., "Thermomechanical Processing and Ductility Enhancement of a 6061 Al- Al_2O_3 Metal Matrix Composite", *Advanced Synthesis of Engineered Structural Materials,* ASM International, Materials Park, Ohio (1992).

8. Schaefer, T. A., *Thermomechanical Processing and Ambient Temperature Properties of a 6061 Aluminum 10 Volume Percent Alumina Metal Matrix Composite,* Master's Thesis, Naval Postgraduate School, Monterey, California, March 1990.

9. Macri, P. D., *Processing Microstructure and Elevated Temperature Mechanical Properties of a 6061 Aluminum-Alumina Metal Matrix Composite,* Master's Thesis, Naval Postgraduate School, Monterey, California, December 1990.

10. Magill, M.D., *The Influence of Thermomechanical Processing Parameters on the Matrix Composite Material,* Master's Thesis, Naval Postgraduate School, Monterey, California, December 1990.

11. Eastwood, D. F., *The Effect of Thermomechanical Processing Parameters on the Ambient Behavior of 10% Volume Al-Alumina,* Master's Thesis, Naval Postgraduate School, Monterey, California, March 1992.

12. Longenecker, F. W., *An Analysis of the Microstructure and Reinforcement Distribution of an Extruded Particle-Reinforced Al 6061-10 Volume Percent Al_2O_3 Metal Matrix Composite,* Master's Thesis, Naval Postgraduate School, Monterey, California, September 1993.

13. Daniel, I., and Isha, O., *Engineering Mechanisms of Composite Materials,* Oxford Press, 1994

14. Clyne, T. W. and Withers, P. J., *An Introduction to Metal Matrix Composites,* Cambridge University Press (1993).

15. Chawla, K. K., *Composite Materials: Science and Engineering,* Springer-Verlag (1987).

16. Lilholt, H., Aspects of Deformation of Metal Matrix Composites", *Materials Science and Engineering,* A135 (1991), pp. 161-171.

17. Meyers, M. A., and Chawla, K. K., *Mechanical Metallurgy: Principles and Applications,* Prentice-Hall, Inc., Englewood Cliffs, New Jersey 07632

18. Hansen, N., *Dispersion Strengthened Aluminum Products-Manufacture, Structure and Mechanical Properties,* Riso National Laboratory, Denmark

19. Singer, A. R. E., "Metal Matrix Composites Made by Spray Forming", *Materials Science and Engineering,* A135 (1991), pp. 13-17.

20. Chadwick, G. A., "Squeeze Casting of Metal Matrix Composites Using Short Fibre Preforms, *Materials Science and Engineering,* A135 (1991), pp. 23-28.

21. Rasmussen, N. W., Hansen, P. N., and Hansen, S. F., "High Pressure Die Casting of Fibre-reinforced Aluminium by Preform Infiltration", *Materials Science and Engineering,* A135 (1991), pp. 41-43.

22. Tweed, J. H., "Manufacture Of 2014 Aluminium Reinforced with SiC Particulate by Vacuum Hot Pressing", *Materials Science and Engineering,* A135 (1991), pp. 73-76.

23. Callister, W. D. Jr., *Materials Science and Engineering: An Introduction,* 3rd ed., John Wiley & Sons, Inc.

24. Fishman, S. G., *Interfacial Science of Structural Composites: Debonding Aspects,* Office of Naval Research, Arlington, Virginia.

25. Nardone, V. C., Strife, J. R. and Prewo, K. M., "Microstructurally Toughened Particulate Reinforced Aluminum Matrix Composites", to be published in Met. Trans.

26. Mortensen, A., Interfacial Phenomena in the Solidification Processing of Metal Matrix Composites, *Materials Science and Engineering,* A135 (1991), pp. 1-11.

27. Leonhardt, G., Kieselstein, E., Podlesak, H., Than, E. and Hofmann, A., "Interface Problems in Aluminium Matrix Composites Reinforced with Coated Carbon Fibres", *Materials Science and Engineering,* A135 (1991), pp. 157-160.

28. Gubbels, G. H. M., "Interfaces in Composites of Alumina in a Molybdenum Matrix", *Materials Science and Engineering,* A135 (1991), pp. 135-139.

29. Lloyd, D. J., "Aspects of Fracture in Particulate Reinforced Metal Matrix Composites", *Acta Metallurgica et Materialia,* Vol. 39, No. 1, (1995), pp. 59-71.

30. Llorca, J., and Poza, P., "Influence of Matrix Strength on Reinforcement Fracture and Ductility in Al- Al_2O_3 Composites", *Materials Science and Engineering,* A185, (1994), pp. 25-37.

31. Wang, B., Janowski, G. M., and Patterson, B. R., "SiC Particle Cracking in Powder Metallurgy Processed Aluminum Matrix Composite Materials", *Metallurgical and Materials Transactions A,* Vol. 26A, (1995), pp. 2457-2467.

32. Singh, P.m., and Lewandowski, J. J., "The Effects of Reinforcement Additions and Heat Treatment on the Evolution of the Poisson Ratio During Straining of Disconinuously Reinforced Aluminum Alloys", *Metallurgical and Materials Transactions A,* Vol. 26A, (1995), pp. 2911-2921.

33. ASM International, *ASM Handbook, Volume 4, Heat Treating*, Prepared under the direction of the ASM International Handbook Committee, (1991).

34. Beckwith, T. G., Marangoni, R. D., and Lienhard V, J. H., *Mechanical Measurements*, 5th Edit., Addison-Wesley Publishing Company, (1993).

35. American Society for Metals, *Metals Handbook, Desk Edition,* American Society for Metals, (1985).

INITIAL DISTRIBUTION LIST

1. Defense Technical Information Center 2
   8725 John J. Kingman Rd., STE 0944
   Ft. Belvoir, VA 22060-6218

2. Dudley Knox Library 2
   Naval Postgraduate School
   Monterey, CA 93943-5101

3. Naval Engineering Curricular Office, Code 34 1
   Naval Postgraduate School
   Monterey, CA 93943-5100

4. Department Chairman, Code ME 1
   Department of Mechanical Engineering
   Naval Postgraduate School
   Monterey, CA 93943-5100

5. Dr. T. R. McNelley, Code ME/Mc 5
   Department of Mechanical Engineering
   Naval Postgraduate School
   Monterey, CA 93943-5100

6. LT Kevin P. Boyle 2
   404 Thornapple Lane
   Libertyville, IL 60048